

1 **Title:** *Sphagnum* peat moss thermotolerance is modulated by the microbiome

2

3 **Authors:** Alyssa A. Carrell ^{a,g}, Travis J. Lawrence ^{a,g}, Kristine Grace M. Cabugao ^b, Dana L. Carper ^a,
4 Dale A. Pelletier ^a, Sara Jawdy ^a, Jane Grimwood ^{d,e}, Jeremy Schmutz ^{d,e}, Paul J. Hanson ^f, A. Jonathan
5 Shaw ^c, David J. Weston ^{a,1}

6

7 **Author Affiliations:** ^a Biosciences Division, Oak Ridge National Laboratory, Oak Ridge, TN, 37831, USA;
8 ^b Bredesen Center for Interdisciplinary Research and Graduate Education, University of Tennessee,
9 Knoxville, TN 37996, USA; ^c Duke University, Durham, NC 27708, USA; ^d HudsonAlpha Institute for
10 Biotechnology, Huntsville, AL 35806, USA; ^e Department of Energy Joint Genome Institute, Lawrence
11 Berkeley National Lab, Berkeley, CA, USA. ^f Environmental Sciences Division, Oak Ridge National
12 Laboratory, Oak Ridge, TN, 37831, USA; ^g These authors contributed equally to this work

13

14 **¹Author for correspondence:**

15 David J. Weston

16 Oak Ridge National Laboratory

17 1 Bethel Valley Rd

18 Bldg. 1507, Rm. 214

19 Oak Ridge, TN, 37831, USA

20 Tel.: +1 865 241 8323

21 westondj@ornl.gov

22

23 **ORCIDs:**

24 A. Jonathan Shaw, shaw@duke.edu, 0000-0002-7344-9955

25 Jeremy Schmutz, jschmutz@hudsonalpha.org, 0000-0001-8062-9172

26 Paul J. Hanson, hansonpj@ornl.gov, 0000-0001-7293-3561

27 Dale A. Pelletier, pelletierda@ornl.gov, 0000-0002-4321-7918

28 David J. Weston, westondj@ornl.gov, 0000-0002-4794-9913

29 Alyssa A. Carrell, carrella@ornl.gov, 0000-0003-1142-4709
30 Travis J. Lawrence, lawrencetj@ornl.gov, 0000-0002-7380-489X
31 Dana L. Carper, carperdl@ornl.gov, 0000-0002-4758-8054
32 Kristine Grace M. Cabugao, kcabuga@vols.utk.edu, 0000-0002-1024-192X
33 Sara Jawdy , jawdys@ornl.gov, 0000-0002-8123-5439
34 Jane Grimwood, jgrimwood@hudsonalpha.org, 0000-0002-8356-8325
35

36 **Classification:** BIOLOGICAL SCIENCES: Environmental sciences
37

38 **Keywords:** microbiome, symbiosis, climate change, moss, peatland, microbiome transfer, synthetic
39 communities

40
41 **Author Contributions:** AAC, TJL, DJW designed research; AAC, TJL, DJW, DAP, SJ, JG performed
42 research; AAC, TJL, KGMC, DLC analyzed data; JS, PJH, AJS, AAC, TJL, DJW, DAP, DLC, KGMC
43 wrote the manuscript.

44
45 This manuscript has been authored by UT-Battelle, LLC under Contract No. DE-AC05-00OR22725 with
46 the U.S. Department of Energy. The United States Government retains and the publisher, by accepting
47 the article for publication, acknowledges that the United States Government retains a non-exclusive, paid-
48 up, irrevocable, world-wide license to publish or reproduce the published form of this manuscript, or allow
49 others to do so, for United States Government purposes. The Department of Energy will provide public
50 access to these results of federally sponsored research in accordance with the DOE Public Access Plan
51 (<http://energy.gov/downloads/doe-public-access-plan>).

52

53 **Abstract**

54 *Sphagnum* peat mosses is a major genus that is common to peatland ecosystems, where the species
55 contribute to key biogeochemical processes including the uptake and long-term storage of atmospheric
56 carbon. Warming threatens *Sphagnum* mosses and the peatland ecosystems in which they reside,
57 potentially affecting the fate of vast global carbon stores. The competitive success of *Sphagnum* species
58 is attributed in part to their symbiotic interactions with microbial associates. These microbes have the
59 potential to rapidly respond to environmental change, thereby helping their host plants survive under
60 changing environmental conditions. To investigate the importance of microbiome thermal origin on host
61 plant thermotolerance, we mechanically separated the microbiome from *Sphagnum* plants residing in a
62 whole-ecosystem warming study, transferred the component microbes to germ-free plants, and exposed
63 the new hosts to temperature stress. Although warming decreased plant photosynthesis and growth in
64 germ-free plants, the addition of a microbiome from a thermal origin that matched the experimental
65 temperature completely restored plants to their pre-warming growth rates. Metagenome and
66 metatranscriptome analyses revealed that warming altered microbial community structure, including the
67 composition of key cyanobacteria symbionts, in a manner that induced the plant heat shock response,
68 especially the Hsp70 family and jasmonic acid production. The plant heat shock response could be
69 induced even without warming, suggesting that the warming-origin microbiome provided the host plant
70 with thermal preconditioning. Together, our findings show that the microbiome can transmit
71 thermotolerant phenotypes to host plants, providing a valuable strategy for rapidly responding to
72 environmental change.

73

74 **Key Words:** *Sphagnum angustifolium*, microbiome, symbiosis, climate change, moss, peatland, bog

75 **Introduction**

76 *Sphagnum* peat mosses are fundamental ecosystem engineers (1, 2), contributing to the construction of
77 bog and peatland systems that occupy just 3% of the global land surface yet store approximately 30% of
78 all soil carbon (3, 4). In boreal regions, *Sphagnum* production can increase with modest warming (5, 6),
79 but these positive effects are not entirely generalizable (7) and are expected to be offset by water stress
80 from surface drying (8) and more extreme warming events (9–11). The competitive success and
81 productivity of this keystone genus is largely dependent on symbiotic interactions with microbial
82 associates (12–14), through which ca. 35% of atmospheric nitrogen fixed by diazotrophic bacteria in the
83 microbiome is transferred to the *Sphagnum* host (15). Currently, however, we lack a basic understanding
84 of how warming influences *Sphagnum*–microbiome interactions and how these interactions influence host
85 acclimation and adaptation to elevated temperature.

86 *Sphagnum* symbiosis is characterized by an intimate association with dinitrogen (N_2)-fixing
87 cyanobacteria on the host cell surface and within water-filled hyaline cells (16–19). Hyaline cells provide a
88 key function for nonvascular mosses, which are incapable of active water transport, and also provide a
89 buffered environment for the microbiome that is less harsh than the external pore water, which is
90 characterized by fluctuating temperature spikes and low pH (2). Phylogenetic evidence suggests that
91 bacterial methanotrophs are also important N_2 -fixing members of the *Sphagnum* microbiome in boreal
92 peat bogs (20–23). These methanotrophs not only fix N_2 but also supply 5–20% of the CO_2 necessary for
93 host photosynthesis as a by-product of methane oxidation (24). In addition to the prominent N_2 -fixing
94 bacteria, *Sphagnum* spp. host a diverse array of heterotrophic bacteria, archaea (12), fungi (12), protists
95 (25, 26), and viral symbionts (27) within a complex food web structure. Results from a whole ecosystem
96 peatland warming experiment indicates that elevated temperatures are associated with changes in the
97 *Sphagnum* microbial community, reduced N_2 fixation (28) and reduced *Sphagnum* biomass production
98 (11). It remains unknown whether the warming-altered microbiome influences host acclimation, growth,
99 and production, and if so, in what manner.

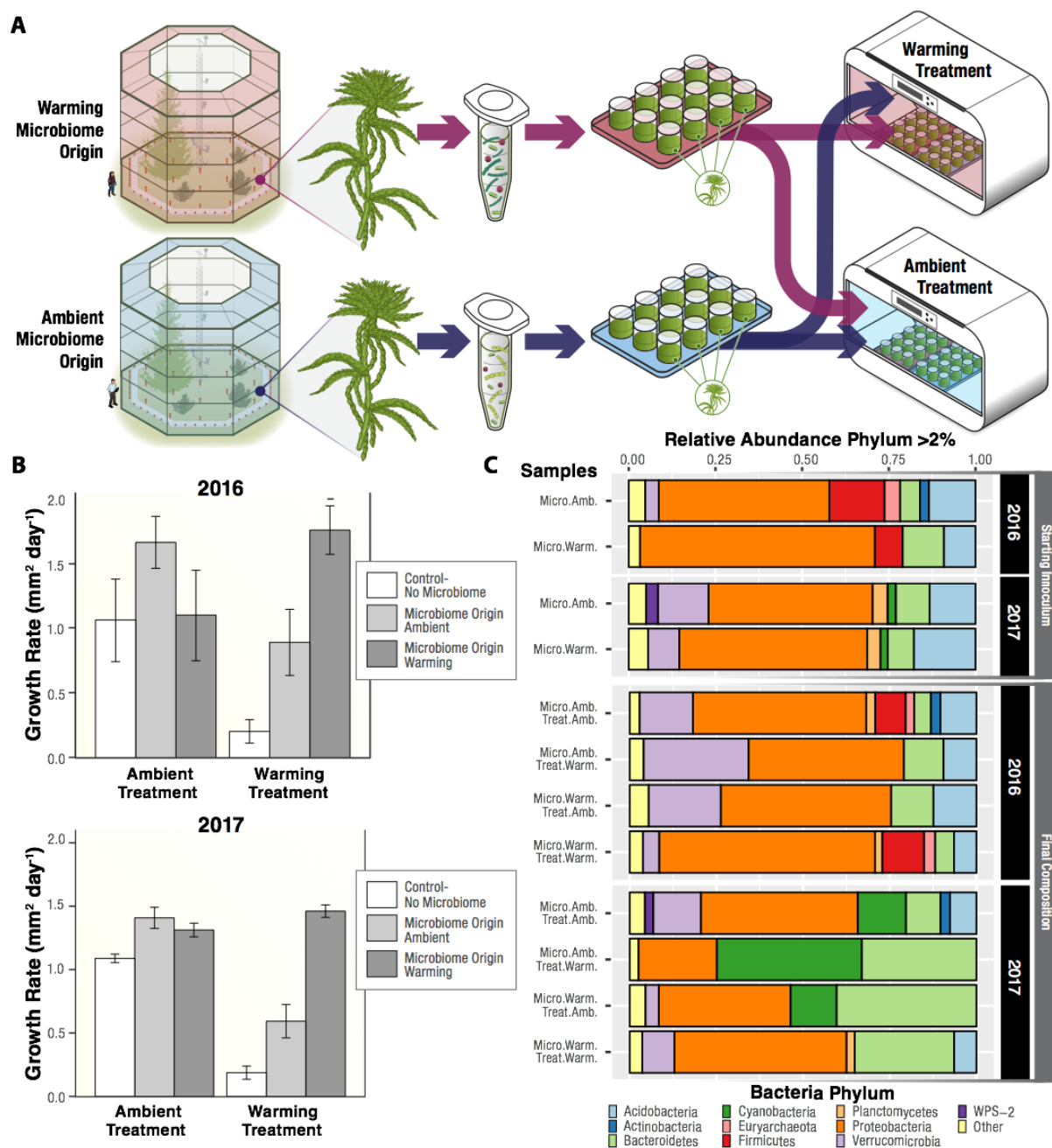
100 Disentangling the effects of *Sphagnum* symbiotic interactions in the context of climate change is
101 thwarted by our inability to predict whether and how mutually beneficial interactions will persist under
102 variable environments. In N_2 -fixing legumes (29) and coral systems (30–33), for example; altered

103 environmental conditions can increase the cost of the interaction relative to the benefits (i.e., the
104 cost:benefit ratio), resulting in breakdown of mutualism and even to antagonistic interactions. One
105 strategy for maintaining a favorable cost:benefit ratio is partner switching, i.e., the substitution of one
106 symbiont for another. In corals, for example, the negative effect of elevated temperatures on host
107 performance can be tempered by replacing symbiont partners with more thermotolerant species (32, 33).
108 By contrast, the habitat-adapted symbiosis paradigm does not emphasize partner choice, but instead
109 proposes that endophytes adapt to stress in a habitat-specific manner and can confer the same functional
110 stress tolerance to their plant hosts (34). Because it is not known whether endophytes are locally adapted
111 or differentiated by environmental sorting, the term “adaptation” is applied loosely (35). Nonetheless,
112 habitat-associated benefits from endophytes originating from extreme temperatures and salinities can
113 benefit host plants subjected to the same environmental extremes (36). By contrast, the habitat origin of
114 fungal endophytes along a rainfall gradient has little effect on the drought responses of *Panicum virgatum*
115 (37). A more explicit test of habitat-associated effects relative to evolutionary history and physiological
116 traits was carried out by Giauque and colleagues (35). They found little support for the idea that fungal
117 endophyte phylogenetic relatedness predicts host benefits, but did find some evidence that microbes that
118 had experienced similarly stressful environments could benefit their hosts. However, the host benefit was
119 not as strong as in previous studies (34), in which fungal endophytes were isolated from more extreme
120 environments. Further complicating the habitat-adaptation paradigm is our lack of understanding of the
121 underlying mechanism or the roles of non-fungal members in conferring host benefits.

122 Given the importance of bacteria for *Sphagnum* performance and ecosystem biogeochemistry
123 (12, 14, 23, 24), we sought to determine the influence of habitat origin on host acclimation to thermal
124 stress. To investigate this experimentally, we mechanically separated the microbiome from field-grown
125 *Sphagnum* plants collected under two extreme thermal conditions, transferred the constituent microbes to
126 germ-free plants, and then exposed the new host plants to short-term heat stress. To assess host and
127 bacterial dynamics, we performed growth analysis, chlorophyll-a fluorescence imaging, metagenomics,
128 metatranscriptomics, and 16S rDNA profiling. The transfer of environmentally conditioned microbiomes to
129 germ-free plants, which is analogous to microbiome transplant studies in medical research, will allow us
130 to (i) determine whether a warming-conditioned microbiome can transmit thermotolerance to the plant

131 host, (ii) characterize the community structure and relative species abundance of beneficial microbiomes,
132 and (iii) allow in-depth exploration of key genes mediating microbially induced host thermotolerance.
133

134 **Results**



135

136 **Fig. 1.** Experimental approach and design: Field-collected donor moss microbiomes collected from
137 ambient or warming conditions were transferred to germ-free recipient moss, and the resulting
138 communities were then placed in an ambient or warm growth chamber (A). Average moss growth rate
139 under ambient or warming treatments, as a function of the thermal origin of the microbiome. Error bars
140 represent standard error of the mean of $n = 6$ for 2016, $n = 12$ for 2017 (B). Relative abundance of
141 microbiome phyla, determined by 16S rDNA amplicon sequencing of the starting field-collected inoculum
142 from ambient or warming experimental plots, and the final compositions of experimental samples (C).

143

144

145 **Plant host performance in response to experimental temperature is dependent on the thermal**
146 **origin of the microbiome**

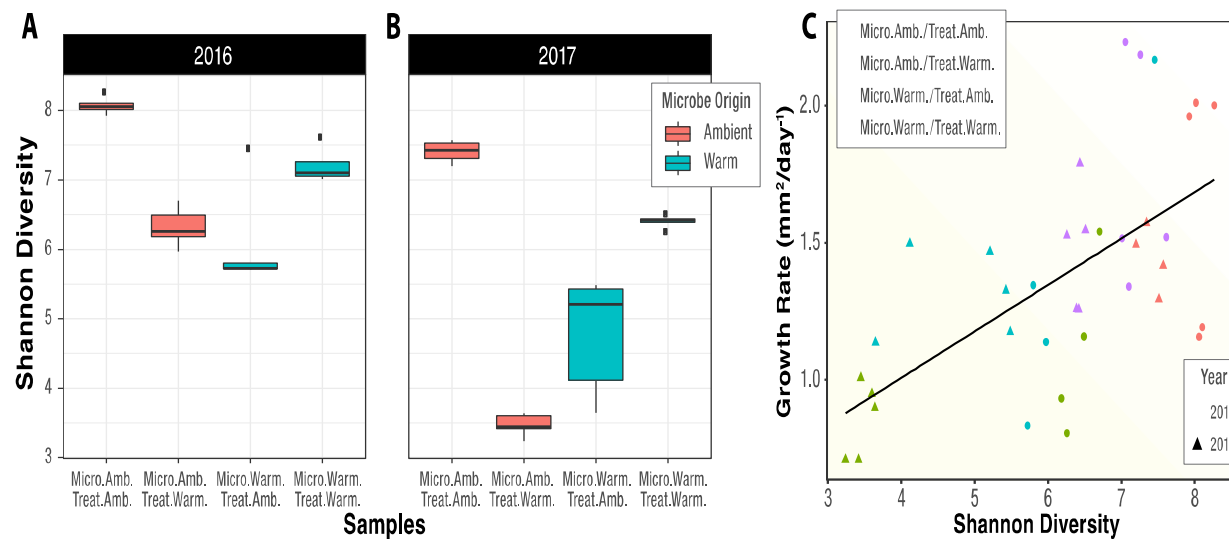
147 In a previous study (28) conducted at a whole-ecosystem peatland manipulation experiment (SPRUCE
148 (38)), we discovered that *Sphagnum*-associated microbiome composition and N₂ fixation were influenced
149 by above- and below-ground warming treatments. To determine the influence of microbiomes from
150 contrasting thermal habitats on plant host thermal acclimation and performance, we conducted
151 microbiome transfer experiments. Starting inocula were isolated from field plants in which we
152 mechanically separated microbes from their *Sphagnum* hosts collected at the SPRUCE experimental field
153 plots exposed to ambient + 0°C (referred to as the ambient microbiome origin) or ambient + 9°C (warming
154 microbiome origin) temperatures Fig. 1A). Independent replicates were collected in two consecutive years
155 (2016 and 2017). Treatments included microbiomes collected from ambient and warming origin
156 conditions, along with a microbiome-free mock control. After transfer of field inocula to laboratory-grown
157 *S. angustifolium*, the constructed communities were exposed to warming or ambient temperature
158 conditions in a full factorial design (Fig. 1A). The repeated 2017 experiment used the same experimental
159 design, except that the number of replicate plants was increased from $n = 6$ to $n = 12$. The microbiome
160 thermal origins were similar to conditions in the experimental chambers (SI Appendix, Table S1).

161 In both years, a donor microbiome that matched the experimental thermal conditions conferred
162 the greatest increase in host growth (Fig. 1B). Host benefits from the microbiome were especially
163 apparent under experimental warming conditions: in 2016 and 2017, moss receiving a warming-origin
164 microbiome exhibited an increase in growth of 87% and 89%, respectively, relative to plants receiving the
165 mock control (Fig. 1B; SI Appendix, Tables 2–4). The addition of a discordant (temperature-mismatched)
166 microbiome increased moss host growth relative to the control by 77% and 68% in the 2016 and 2017
167 experiments, respectively, although post-hoc tests were not significant within year at a $P < 0.05$ alpha
168 level. Generally, benefits to plant host were most pronounced under experimental warming conditions,
169 under which plants without microbes were severely affected (Fig. 1B). Host benefits from temperature-
170 mismatched microbiomes were least prominent under ambient experimental treatment, in which growth

171 increases ranged from 3 to 17% following inclusion of a warming-origin microbiome ($F_{\text{temperature:microbiome}} =$
172 32.01; $P < 0.05$ for 2017; *SI Appendix, Table 3*). Throughout the experiment, moss photosynthetic activity
173 and response to temperature and microbiome origin were evaluated by monitoring chlorophyll-a
174 fluorescence (F_v/F_m). The results mirrored the growth analysis: F_v/F_m values were higher when
175 microbiome thermal origin matched experimental temperature (*SI Appendix, Table S5-6 & Fig. S1-2*).
176 Thus, the warming microbiome consistently increased moss performance to warming, as reflected by
177 growth rate and photosynthetic activity, demonstrating that microbiome thermal origin can play a
178 substantial role in host moss acclimation to elevated temperatures.

179

180 **Habitat origin and thermal treatment conditions structure the starting microbiome and resultant**
181 **microbial community**



182

183 **Fig. 2.** Shannon diversity index of the microbiome at the conclusion of the experiments in 2016 (A) and
184 2017 (B), based on 16S rDNA amplicon data. Microbiomes were less diverse when the thermal origin and
185 experimental treatment were mismatched (i.e., Ambient Origin in Warming Treatment or Warming Origin
186 in Ambient Treatment). Plant growth rate was linearly correlated with microbiome Shannon diversity at the
187 conclusion of the experiment (C).

188

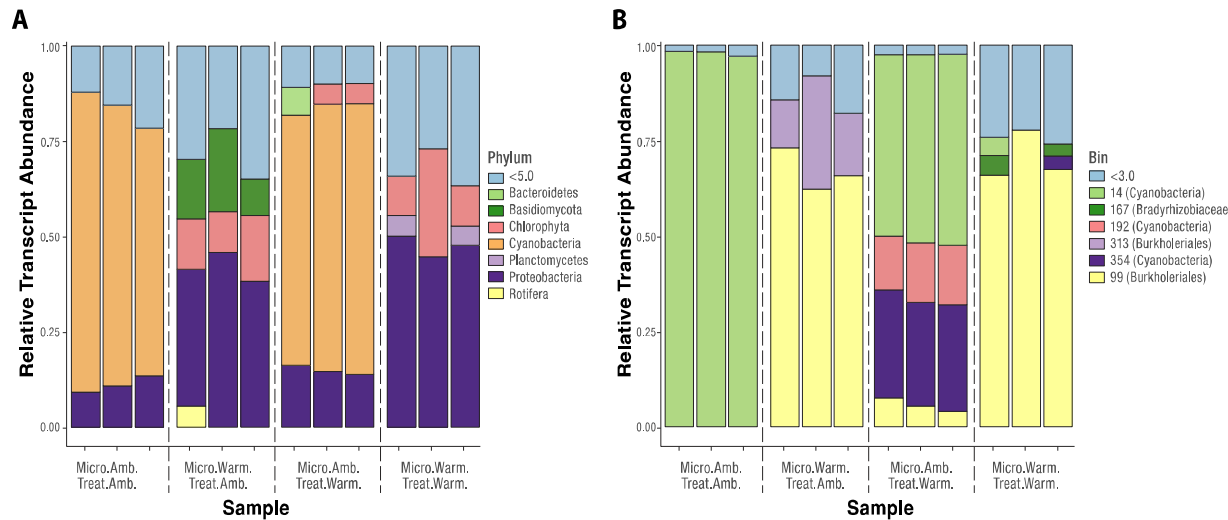
189 In 2017, the initial community structure of the *S. angustifolium* field-collected inoculum differed between
190 thermal origins (Adonis, $R^2 = 0.92133$, $P = 0.009$) and 2016 (Adonis, $R^2 = 0.53$, $P = 0.1$) (*SI Appendix, Fig*
191 *S3*). At the class level, the ambient-origin microbiome consisted largely of Alphaproteobacteria (32%)

192 and Clostridia (16%) in 2016, whereas Alphaproteobacteria (30%) and Acidobacteria (11%) were most
193 abundant in 2017 (*SI Appendix, Table S7*). Within the warming-origin microbiome, Gammaproteobacteria
194 were highly abundant in 2016 (43%), but only constituted 15% of community abundance in 2017, with the
195 difference compensated by an additional increase in Alphaproteobacteria abundance (30%). Despite
196 between-year differences in community composition at the class level within thermal regimes, the growth
197 benefits provided to the plant were strikingly consistent (Fig. 1B).

198 *Sphagnum*-associated microbial communities responded to four weeks of thermal treatment
199 conditions regardless of year, thermal origin, or growth temperature. Non-metric multidimensional scaling
200 (NMDS) ordinations of the microbiome Bray-Curtis distance matrix revealed that the community
201 composition of the warming-origin microbiomes responded similarly across thermal treatments, whereas
202 ambient-origin microbiome structure varied to a greater extent both across and within thermal treatments
203 (*SI Appendix, Fig S4*). To determine whether changing community composition influenced microbial
204 diversity, we estimated the Shannon diversity index for each treatment condition at the conclusion of the
205 study in both years (Fig. 2A–B). Microbial diversity was highest when microbiome thermal origin matched
206 chamber treatment temperatures; conversely, discordant combinations resulted in substantially lower
207 microbial diversity (Fig. 2A–B). The ambient-origin microbiome had the highest diversity under matched
208 (i.e., ambient) treatment conditions in both years (ANOVA, $P < 0.01$). Similarly, the warming-origin
209 microbiome had the highest diversity under the warming treatment in both years (ANOVA, $P < 0.01$).
210 Detailed class-level community composition assignments are provided in *SI Appendix, Table S8*. Given
211 that greater phylogenetic diversity is likely to be accompanied with greater metabolic and functional
212 diversity, we hypothesized that microbial diversity would be associated with enhancements in plant
213 acclimation to stressful warming conditions, reflected by improved growth. Providing correlative support
214 for this hypothesis, bacterial and archaea diversity (as inferred from 16S rDNA) at the end of the
215 experiment was correlated with *Sphagnum* growth (Pearson correlation, $r = 0.744$, $p=0.003$; Fig.2B). By
216 contrast, ITS-derived fungal diversity estimates did not correlate with moss growth (Pearson corr., $r = -$
217 0.204, $P = 0.403$; *SI Appendix, Fig S5*), and indeed the fungal communities did not vary greatly across
218 treatments (*SI Appendix, Table S9-10*), therefore we largely focused on the bacterial component of the
219 microbiome in proceeding sections.

220

221 **Metagenome and metatranscriptome analyses reveal changes in symbiotic *Cyanobacteria***
222 **abundance and composition, and host plant transcriptional reprogramming in response to**
223 **temperature treatment**



224

225 **Fig. 3.** Relative abundance of microbial transcripts mapping to metagenome contigs for (A) major phyla
226 and (B) metagenome-assembled genomes (MAGs). Each bar represents a metatranscriptome sample for
227 the ambient-origin (Micro.Amb.) or warming-origin (Micro.Warm) microbiome under either the ambient
228 (Treat.Amb.) or warming (Treat.Warm) treatment. Colors indicate (A) phyla or (B) MAGs; light blue
229 represents (A) phyla with <5% or (B) MAGs with <3% of mapped transcripts.

230

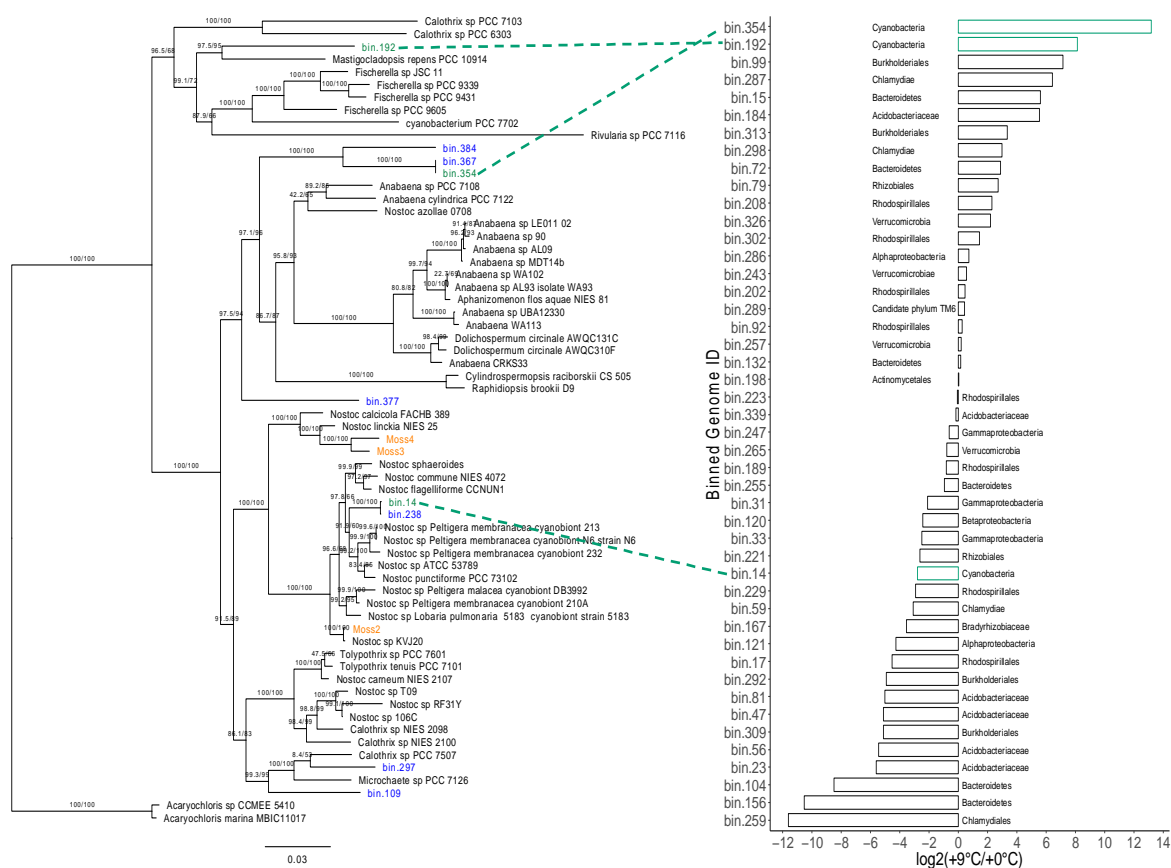
231 Host thermal acclimation and productivity varied with microbiome origin. To further explore how
232 community dynamics influence host thermal acclimation, we used metagenomics and
233 metatranscriptomics to identify both plant and microbial gene sets responsive to thermal and microbiome
234 conditions (Fig. 3). For metagenome assemblies, DNA sequencing reads mapping to the *S. angustifolium*
235 genome (https://phytozome-next.jgi.doe.gov/info/Sfallax_v1_1) were removed, and the remaining reads
236 were co-assembled into 4,762,069 contigs with an N50 of 1261 bp. Binning of metagenome contigs
237 yielded 45 metagenome-assembled genomes (MAGs) with a quality score ≥ 70 with $\leq 5\%$ contamination
238 (SI Appendix Supplemental Table S11). The high-quality MAG standard of $>90\%$ complete and $<5\%$
239 contamination (39) was met for 28 of our genomes, whereas 13 and 9 MAGs are $>95\%$ and $>97\%$
240 complete, respectively. Taxonomic assignments and blast hits from annotated proteins were resolved to

241 the lowest taxonomic level using CheckM (40) and DIAMOND (41) (*SI Appendix, Table. S11*). For
242 metatranscriptomes, we generated 429.6 GB of RNA-seq data across three replicates for each treatment.
243 On average, 40.93 million (M) \pm 7.39 M reads passed quality filtering per sample across all thermal
244 treatments and microbiome conditions (*SI Appendix, Table. S12*). In samples derived from plants
245 receiving a microbiome transfer, approximately 65% of reads aligned to the *Sphagnum* genome, except in
246 the discordant case when plants received ambient-origin microbiomes followed by warming treatment.
247 Under that condition, the plants were severely stressed, and only 12.4% of the reads aligned to the
248 *Sphagnum* genome (*SI Appendix, Fig. S6*).

249 To expand on the amplicon-based community composition results (Fig. 1C, *SI Appendix, Table*
250 *S7*) and determine which microbial members are transcriptionally active, we categorized transcriptional
251 profiles based on taxonomic composition. Under matched ambient origin and experimental temperature,
252 microbial transcripts were mostly from Cyanobacteria symbionts (72.5 \pm 6.9%), followed by
253 Proteobacteria (11.2 \pm 2.2%) (Fig. 3A). Under matched warming origin and temperature treatment,
254 Cyanobacteria transcript reads were largely absent, and the metatranscriptome was mainly derived from
255 Proteobacteria (47.5 \pm 2.7%), Chlorophyta (16.39 \pm 10.4%), and Planctomycetes (4.9 \pm 0.57%). Results from
256 mismatched origin and experimental conditions more closely reflected their microbiome origin
257 communities (*SI Appendix, Table S7*). This finding was also reflected in a multidimensional scaling
258 analysis using level 3 SEED functional annotation, in which cluster variation was explained more on
259 microbial origin rather than experimental temperature (*SI Appendix, Fig. S7*).

260

261 **Experimental warming increases transcript abundance from alternative cyanobacteria members,**
262 **signaling possible symbiont exchange**



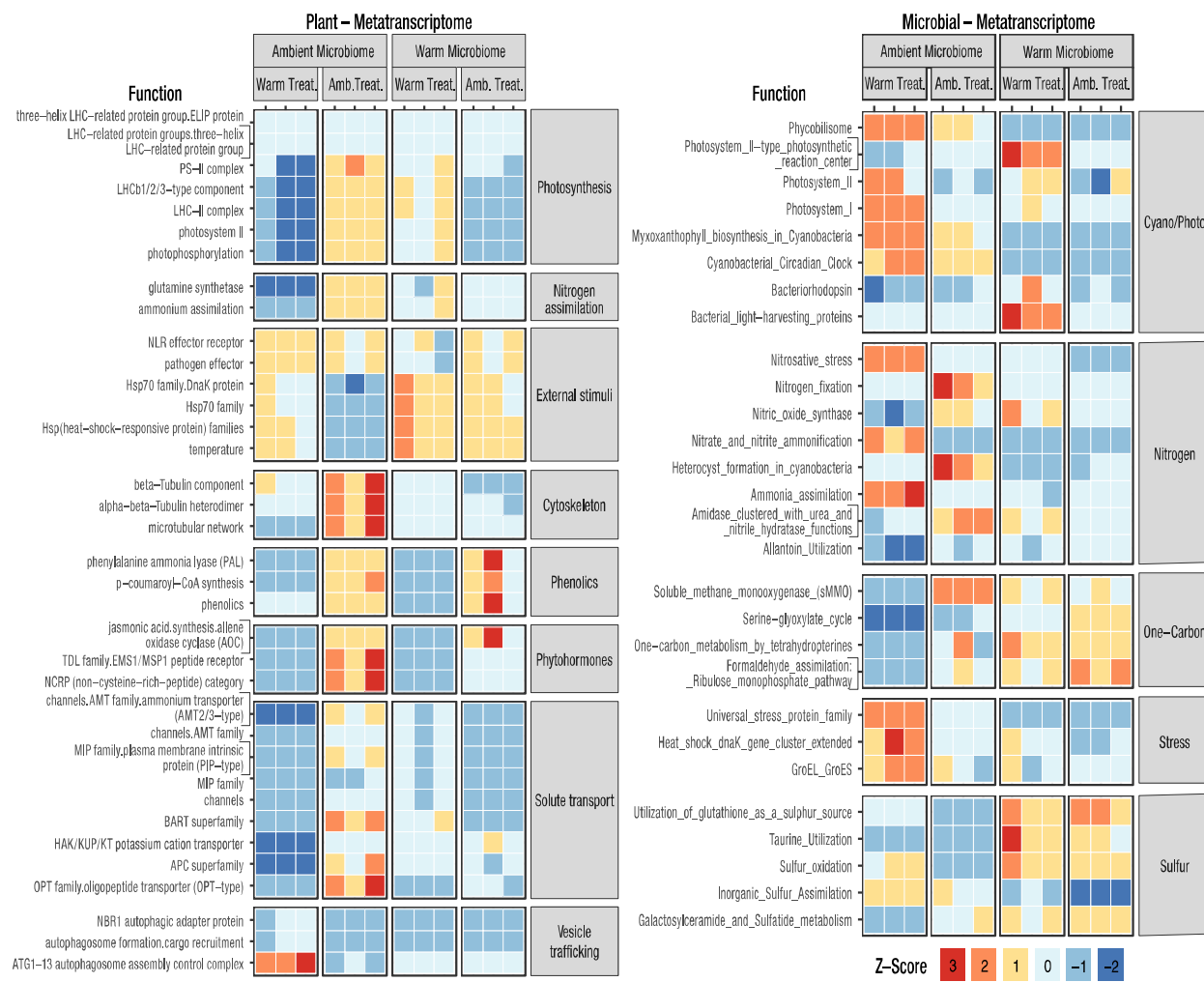
263
264 **Fig 4. Phylogeny of select Cyanobacteria and log₂(fold change) of metagenomic bins. (A) Maximum-**
265 **likelihood phylogram where the numbers at nodes indicate UFBoot2 and SH-like approximate likelihood**
266 **ratio support. Branch lengths indicate estimated substitutions per site. Metagenomic bin taxa labels are**
267 **colored by source within SPRUCE enclosures (green), outside SPRUCE enclosures (blue), or from (42)**
268 **(orange). (B) Bar chart representing log₂(fold change) of metagenomic bins between ambient-origin and**
269 **warming origin metagenomes. Green bars indicate cyanobacterial MAGs recovered in this work.**

270
271 Differences in the composition and abundance of *Sphagnum*-associated cyanobacteria in response to
272 warming are important because these organisms are key symbionts with *Sphagnum* mosses, and the
273 exchange of symbionts with more thermotolerant forms has been implicated in host thermotolerance in
274 coral systems (e.g., 34). To explore this further, we taxonomically refined three of our high-quality
275 cyanobacteria MAGs with a phylogenetic tree reconstruction using an additional 109 cyanobacterial
276 genomes (Fig. 5). We found that all three cyanobacterial MAGs belong to the heterocystous B1 clade of
277 Cyanobacteria, which also contains known plant associates (43). To determine which of the
278 cyanobacteria are most responsive to thermal conditions, we aligned the microbial RNA-seq reads from

279 the end of the experiment onto the MAGs. Of all non-*Sphagnum* RNA-seq reads, $31.6\pm8.7\%$ mapped
280 onto cyanobacteria MAGs for matched ambient-origin and ambient temperature conditions. This
281 percentage decreased to $26.1\pm1.1\%$ when plants receiving ambient-origin microbiomes were subjected to
282 discordant warming treatment. Further, microbiomes originating from warming field conditions contained
283 negligible levels of cyanobacterial RNA-seq reads (0.1–0.08%). Cyanobacterial reads predominantly
284 aligned to MAG bin 14 ($98\pm0.7\%$), but to a considerably lesser extent ($49\pm0.6\%$) when placed under
285 warming experimental conditions. The decrease in bin 14 RNA-seq reads was accompanied by an
286 increase in reads from *Cyanobacteria* bins 354 ($28\pm0.6\%$) and bin 192 ($15\pm0.9\%$) (Fig. 3B). Due to
287 sampling constraints, we did not normalize the results of RNA-seq analysis to community abundance
288 changes. Nonetheless, in light of abundance estimates based on metagenomic data (Fig. 3), field-
289 collected 16S rDNA amplicon results from this study (Fig. 1), and results of a prior study (26), we are
290 confident that warming decreases the abundance of *Sphagnum*-associated cyanobacteria and changes
291 cyanobacterial membership of the community.

292

293 **Host plant transcriptional reprogramming and acclimation in response to warming are
294 consequences of microbiome thermal origin**



295

296 **Fig 5.** Heatmap of z-scores for (A) MapMan4 ontology categories enriched in differentially expressed
 297 plant genes and (B) differentially expressed SEED level 3 categories related to nitrogen, one-carbon, and
 298 sulfur metabolism; cyanobacterial/photosynthesis; and stress. Differential expression was defined as
 299 $|\log_2(\text{Fold Change})| > 1$ and corrected $p < 0.05$.

300

301 Given that the warming environment alters community composition in a way that benefits host plant
 302 acclimation to warming, we hypothesized that the warming environment selects for more thermotolerant
 303 symbionts that are able to maintain nitrogen exchange with the plant at elevated temperatures. If this is
 304 the case, we would expect that plant and microbial transcriptional patterns relating to N transport and
 305 metabolism would be similar between matched origin and temperature conditions (i.e., warming origin +
 306 warming treatment or ambient warming + ambient treatment). Functional ontology enrichment analysis
 307 across all conditions revealed that in plants receiving an ambient-origin microbiome and ambient

308 treatment condition, gene expression was enriched for pathways involved in N metabolism, including
309 ammonium transporters, ammonium assimilation, and glutamine synthetase, as well as growth-related
310 ontologies including photosynthesis, cytoskeletal elongation, and hormonal regulation (Fig. 4A). This was
311 also apparent on a \log_2 (fold change) (LFC) basis when comparing plants with an ambient-origin
312 microbiome between temperature conditions (*SI Appendix, Dataset S1*). In this case, ambient treatment
313 plants corroborated enrichment analysis with induced ammonium transport (LFC 4.0, $P = 2.0 \times 10^{-2}$) and
314 glutamine synthetase (LFC 2.4, $P = 1.1 \times 10^{-2}$). In addition, 153 of 178 genes within the photosynthesis
315 ontology were induced, with photosystem II light-harvesting complex II most strongly affected (LFC 2.1, P
316 $= 2.48 \times 10^{-6}$). In addition, we noted differences in fatty acid synthesis, especially in desaturation and
317 elongation (LFC 2.74, $P = 2.97 \times 10^{-6}$), phenolic secondary metabolite production (LFC 2.86, $P = 1.77 \times$
318 10^{-5}), cell wall expansion (LFC 6.5, $P = 2.7 \times 10^{-6}$), phytohormone signaling with non-cysteine-rich
319 peptides (LFC 4.63, $P = 8.1 \times 10^{-4}$), jasmonic acid synthesis (LFC 2.36, $P = 4 \times 10^{-2}$), and response to
320 external stimuli (LFC 2.53, $P = 3.2 \times 10^{-2}$). As expected, heat shock proteins (HSPs) were responsive to
321 warming, especially the HSP70 family, of which 15 members were induced (LFC 1.2, $P = 6.5 \times 10^{-3}$).

322 Plant ontology enrichment analysis did not support the hypothesis that the warming-origin
323 microbiome would provision the plant with N at warming treatment conditions (Fig. 4A). Likewise, there
324 was no support for this hypothesis on an LFC basis when comparing RNA-seq profiles from plants with
325 warming-origin microbiomes across temperature treatments (*SI Appendix, Dataset S1*). Despite the
326 apparent lack of microbially provided fixed N, the warming-origin microbiome still provided growth benefits
327 to warming-treated plants (Fig. 1B), and this was also apparent in RNA-seq enrichment analysis of
328 growth-related ontologies. Specifically, plants exposed to warming that received warming-origin microbes
329 exhibited enrichment for photosynthesis - photosystem II light harvesting complex II (LFC 1.4, $P = 1.9 \times$
330 10^{-3}), cell wall expansion (LFC 2.5, $P = 1.3 \times 10^{-5}$), and phenolic secondary metabolite production (LFC
331 $2.9, P = 2.0 \times 10^{-8}$).

332 Microbial RNA-seq differential expression (DE) analysis of functional ontologies supported the
333 notion that the warming-altered cyanobacteria community is not fixing N, and is therefore not provisioning
334 the plant with N. DE enrichment analysis revealed that microbial N metabolism differed dramatically
335 between both treatments and origins (Fig. 4B, *SI Appendix*, Table S13). Indeed, exposure to warming

336 decreased N-fixation ontology gene expression by 53.4-fold (Fig. 5B, *SI Appendix*, Table S13). Moreover,
337 there was no enrichment evidence for N-fixation among the warming-origin microbiomes, regardless of
338 temperature treatment. Although we could not obtain direct evidence for N-fixation in this study due to
339 sample size restrictions, these observations corroborate prior $^{15}\text{N}_2$ -based fixation rates reported at the
340 same field site where our warming- and ambient-origin inocula were obtained (28).

341 How the warming-origin microbiome influences host plant photosynthesis and growth temperature
342 acclimation remains to be elucidated, but we can glean clues from communities composed of discordant
343 warming-origin microbes at ambient experimental temperatures. In that case, enrichment for the HSP70
344 family and phenolic compounds are induced without heat (Fig. 4A). This trend was also observed on a
345 LFC basis where 33 out of 35 detected HSPs were induced (*SI Appendix, Dataset S1*). This suggests that
346 the warming-origin microbiome is eliciting, or preconditioning, the host plant heat shock response without
347 the need for elevated temperatures.

348

349 **Discussion**

350 The establishment of constructed communities derived from microbiome transfers, coupled with
351 comparative metatranscriptomics, revealed several novel aspects of microbial contributions to plant
352 temperature response. First, plants receiving a microbiome from a high-temperature environment
353 exhibited enhanced photosynthetic and acclimation responses to similarly warm environments. Second,
354 the warming-origin microbiome was less diverse than the ambient field-collected microbiome, but
355 contained transcripts from a more diverse set of cyanobacteria, suggesting symbiont swapping or
356 replacement. Finally, the warming-origin microbiome transferred a thermotolerant phenotype to the plant
357 through the induction of host genes involved in the heat shock response and hormonal regulation.

358 Our results demonstrate that the originating thermal habitat of the microbiome has a dramatic
359 effect on *Sphagnum* host acclimation to elevated temperatures. These results were consistent across two
360 years of field-collected donor inocula and two independent laboratory experiments. Although the fact that
361 plants benefit from microbial relationships is well known, the transfer of microbially acquired habitat
362 specific tolerance to recipient plants was reported much more recently, and to date has been limited to
363 endophytic fungi (44). In an early example of this, Redman et al. (45) collected a native north American

364 grass, *Dichanthelium lanuginosum*, endemic to geothermal sites with soil temperatures reaching up to
365 50°C . After isolation of a *Curvularia* sp. fungus and re-inoculation onto endophyte free plants,
366 thermotolerance was conferred to the recipient plant host. This approach of isolating endophytic fungi
367 from plants endemic to extreme habitats in an attempt to confer habitat-associated benefits has been
368 tested a number of times with both successful (34, 36) and mixed results (35, 37). In all cases, the
369 microbial component focused on fungi and was constrained to single member strain-based studies.

370 The microbiome transfer approach used in this study allowed us to test habitat-associated
371 benefits from a broader set of organisms that is more representative of the dynamic coevolving
372 community. However, this strategy made it difficult to relate specific taxa to recipient host benefits. For
373 example, the warming-origin inocula differed substantially between years, even at the phylum level, yet
374 both provided host thermal benefits. This is consistent with the idea that microbial community taxonomic
375 composition is not necessarily a clear indication of community function. Indeed, functional similarity
376 independent of taxonomic group has been reported in other systems, including human gut (46) and
377 microalgae (47) microbiomes. Hence, the challenge is to look beyond taxonomic association and
378 determine what components of the microbiome are responsible for conferring thermotolerance on the
379 host plant.

380 One possible mechanism for enhanced host temperature tolerance is the replacement of primary
381 symbionts with more thermotolerant symbionts. *Sphagnum* mosses have long been known to host N₂-
382 fixing Cyanobacteria as symbionts (16–19). More recently, they have been shown to associate with a
383 suite of bacteria, including those that oxidize methane into CO₂, as well as a number of viral, archaea,
384 and protists (reviewed in (12)). The influence of warming on these symbionts, especially the
385 Cyanobacteria, would directly affect host nutrient status and productivity. Our metagenome analysis in
386 this study assembled three Cyanobacterial MAGs. DNA and RNA-seq reads mapping to the binned MAG
387 genomes indicated that *Sphagnum* plants were primarily colonized by a single Cyanobacterial member
388 from genus *Nostoc*. With increasing temperature, this *Nostoc* MAG decreased abundance, while two
389 additional Cyanobacterial MAGs are increasing in abundance, indicating a possible exchange for more
390 thermotolerant members of the clade. Precedent for symbiont shuffling has been provided in coral
391 systems. Coral host algal symbiont communities that are genetically diverse and susceptible to symbiont

392 loss due to environmental stress and ensuing coral bleaching events. However, the stress events leading
393 to the bleaching, as well as the bleaching itself, provide an opportunity for replacement of symbionts with
394 organisms that are more suitable to the new environmental condition, such as those with higher stress
395 tolerance (reviewed in (48)). The coral system also demonstrates the potential role of the surrounding
396 bacterial community in coral thermotolerance. This was elegantly demonstrated by Ziegler and colleagues
397 (49), who showed that long-term temperature elevation modified the composition of the bacterial
398 community, and that particular bacterial taxa could predict coral thermotolerance. However, the coral
399 system is not amenable to germ-free host strains or microbiome transfers, making it difficult to quantify
400 the contribution of the microbiome to host thermotolerance.

401 From the results of this study, it is difficult to discern whether host thermal benefits from the donor
402 microbiome are driven by community change from primary *Nostoc* Cyanobacteria symbionts, or instead
403 by the surrounding microbial community. Our hypothesis that the key cyanobacteria symbiont was
404 augmented by additional thermotolerant cyanobacteria in order to maintain N₂ fixation at elevated
405 temperatures was not entirely supported. Although we observed an increase in cyanobacteria diversity,
406 and thus possible evidence for exchange with thermotolerant symbionts, the metatranscriptome analysis
407 yielded no evidence for N₂-fixation under warming. This is consistent with a prior field study (28) at the
408 same SPRUCE site, where 16S rDNA amplicon profiling, *nifH* qRT-PCR, and ¹⁵N₂ incubation assays
409 revealed a decrease in *nifH*-containing N-fixing bacteria and a reduction in ¹⁵N₂ incorporation in response
410 to warming.

411 Despite the lack of evidence for a contribution of N₂-fixation in contributing to plant
412 thermotolerance, the metatranscriptome analysis did reveal a role for host plant heat shock
413 reprogramming. Plants that never received a warming treatment were enriched for Hsp70 gene family
414 transcripts when they received a warming-origin microbiome, but not when they received an ambient-
415 origin microbiome. The Hsp70 family is often associated with thermotolerance: multiple studies have
416 reported that thermotolerance is decreased by Hsp70 antisense and increased by Hsp70 overexpression
417 (50). It should be noted that our metatranscriptome analysis did not show microbial-mediated repression
418 of the Hsp90 family or induction of the Hsp101 family, both of which have been implicated in the heat
419 shock response. Microbially mediated repression of *Arabidopsis* Hsp90, leading to elevated

420 thermotolerance, was previously demonstrated in the desert-dwelling fungus *Paraphaeosphaeria*
421 *quadrisepata* (51).

422 In addition to Hsp70 reprogramming, the warming-origin microbiome elicited host plant
423 expression of genes contributing to jasmonic acid synthesis (*via* allene oxide cyclase [AOC]). Jasmonic
424 acid is a key phytohormone contributing to both abiotic and biotic stress responses, and has been
425 implicated in flowering plant thermotolerance (52). AOC synthesizes 12-Oxo-phytodienoic acid (OPDA),
426 which is a signaling compound and intermediate in the jasmonic acid biosynthesis pathway. In the
427 liverwort *Marchantia polymorpha*, overexpression of AOC increases OPDA, suggesting that its function is
428 similar to that of its homologs in flowering plants (53). However, AOC overexpression in *M. polymorpha*
429 decreases growth. Likewise, the warming-origin microbiome induced expression of enzymes involved in
430 the production of phenolic compounds, including phenylalanine ammonia lyase (PAL), which has been
431 implicated in both temperature response and disease resistance (54). In contrast to the heat shock
432 response, the jasmonic acid and phenolic ontology enrichments disappeared after the plants were
433 exposed to warming. It remains to be determined whether these compounds are contributing to a
434 beneficial thermal preconditioning or instead reflect a defensive response.

435 One unexpected observation was that the warming-origin microbiome elicited the induction of the
436 heat shock response in plants that were never exposed to elevated temperatures. Thermotolerance can
437 be acquired by prior exposure to a sublethal temperature stress (55). Similarly, plants associated with
438 beneficial rhizosphere microbes can more rapidly mount a defense response to biotic and abiotic
439 stressors (56). Although there is a considerable body of literature on the biotic aspects of microbial-
440 induced plant priming, increasing evidence suggests that plants can also be primed against abiotic
441 stressors. For example, Ali et. al (57) found that a *Pseudomonas* sp. strain isolated from pigeon pea
442 endemic to an arid region conferred enhanced survival and growth on sorghum seedlings exposed to
443 elevated temperatures. This early example has been corroborated with multiple plant hosts and microbial
444 strains, yet the underlying genetic mechanisms remain to be identified (53 and citations within). In most
445 cases studied thus far, microbial-induced resistance to abiotic stress has been studied in individual
446 strains or small community consortia. By contrast, in this study we examined how microbial dynamics
447 within large communities interact to influence host physiology and growth.

449 **Conclusions**

450 Our findings provide a starting point for future studies that systematically decouple inherent host
451 acclimation responses to challenging environmental conditions from those of the associated microbiome.
452 A key benefit of the microbiome transfer and constructed community approaches described here is that it
453 allows the coevolved host–microbiome consortia collected from extreme environmental conditions to be
454 separated and tested across a range of thermal experimental conditions. Our observation that the
455 microbiome can transmit thermotolerant phenotypes has a number of implications. It sets the stage for
456 moving beyond the current notion that plants are restricted to “adapt or migrate” strategies for survival to
457 rapidly changing environmental conditions (59). The current study provides an alternative perspective on
458 these outcomes by showing that thermotolerant phenotypes can be rapidly transmitted to plant host. We
459 anticipate multiple challenges as the findings of our studies are transferred beyond the laboratory into
460 ecological systems. First, additional research is needed to determine the extent to which inter- and intra-
461 specific genetic variation influences the plant’s ability to receive microbial benefits, and if so, identifying
462 the causal alleles. Bringing this goal closer to reality, a genome sequencing campaign representing some
463 55 species within the approximately 300-member *Sphagnum* genus, as well as the development of high-
464 density genetic maps from sequencing of a 200-member pedigree cross, are currently underway (60).
465 Second, the identification of responsible microbial taxa is challenged by large community diversity,
466 complex community interactions and strain isolation limitations. These experimental tests could take
467 multiple forms, from the dilution and sequencing of donor microbiomes to strain isolation and testing in
468 our demonstrated plate-based experimental system. Within the context of this study, such an approach
469 could determine whether microbial benefits are mainly a function of swapping primary cyanobacteria
470 symbionts for more thermotolerant members, or whether additional microbial members are driving the
471 host phenotype. Finally, determining the impact of plant host-microbiome interactions within the context of
472 competition poses a major challenge. For example, is the evolution of mutualistic interactions a key driver
473 in *Sphagnum* versus vascular plant competition? If so, how does changing environmental conditions
474 influence these mutualistic interactions within a competitive framework, and how does that scale to alter
475 peatland C and nutrient cycling dynamics across regional and global scales (61, 62)?

476

477 **Materials and Methods**

478

479 **Study site and field sampling**

480 The Spruce and Peatland Responses Under Changing Environments (SPRUCE) experiment, located in
481 the S1 bog of the Marcell Experimental Forest (47° 30.4760' N; 93° 27.1620' W; 418 m above mean sea
482 level), MN, USA, employs a regression-based design at the whole-ecosystem scale to produce nominal
483 warming of ambient +0°C, +2.25°C, +4.5°C, +6.75°C, and +9°C in a *Picea mariana*–*Sphagnum* spp.
484 raised bog ecosystem with open-top chamber systems (38). Heating of the soil was initiated in June 2014
485 and aboveground air heating began in June 2015. A full discussion of experimental details and
486 ecosystem description is available (38). To obtain field-conditioned microbiomes, living green stems of
487 *Sphagnum* were collected from ambient + 0°C (ambient) and ambient + 9°C (elevated) plots in August
488 2016 and August 2017. The collected stem portion typically included capitula and 2-3 cm of living stem.
489 The *Sphagnum* material was placed in sterile bags and shipped to Oak Ridge National Laboratory on
490 blue ice.

491

492 **Isolation of microbiomes, application to gnotobiotic *Sphagnum*, and warming treatment**

493 To isolate the microbiomes from the field samples, 100 g of tissue was diced with a sterile razor blade
494 and pulverized in PBS with a mortar and pestle. The resulting suspension was filtered through Mira Cloth,
495 centrifuged to pellet the microbes, and then resuspended in 500 ml BG11 -N medium (pH 5.5). A single
496 capitulum of axenic *Sphagnum angustifolium* was added to each well of a 12-well plate and inoculated
497 with 2 ml of ambient-origin microbiome, warming origin microbiome, or sterile media. *Sphagnum*
498 *angustifolium* genotype was the same genotype that was sequenced by the DOE JGI ([https://phytozome-
499 next.jgi.doe.gov/info/Sfallax_v1_1](https://phytozome-next.jgi.doe.gov/info/Sfallax_v1_1)). The plates were placed into growth chambers with a 12hr:12hr
500 light:dark cycle, programmed to either ambient or elevated field plot temperatures. June 2016 field plot
501 temperatures from 6-hour blocks were averaged from each day, resulting in a cycle of 4 temperatures.
502 June 2017 temperatures did not differ from those in June 2016, so the same temperature profile was
503 used for incubations for both years (SI Appendix, Table 1).

504

505 **Measurement of growth and photosynthesis**

506 To measure growth, black and white images were collected weekly, and surface area was measured
507 using the ImageJ software (63). Change in surface area was determined as a proxy for growth. To
508 estimate maximal PSII quantum yield, chlorophyll fluorescence parameters were measured weekly with a
509 FluorCam FC800 (PSI, Bruno, Czech Republic) after a 20-minute dark adaptation. Maximum quantum
510 yield (QY_max) was determined using the FluorCam 7 software.

511 Normality of data was checked using the Shapiro-Wilke's test prior to checking homoskedasticity
512 of variances using Levene's Test in the R package 'car' (64). Growth rate (mm day⁻¹) and total growth
513 over the duration of the experiment were rank-transformed prior to two-way ANOVA to assess the
514 influence of experimental temperature and donor microbiome. Fluorescence (Fv/Fm) was measured in
515 moss as a proxy for photosynthetic activity throughout the experiment. However, to highlight the greatest
516 differences in donor microbiome and experimental temperature combinations, only fluorescence data
517 from the last week were used. Fluorescence data was also rank-transformed prior to using a two-way
518 ANOVA. $\alpha=0.05$ was used to denote statistical significance in both two-way ANOVA and Tukey's HSD
519 post-hoc analyses. Growth and fluorescence statistics were analyzed using R version 3.5.1 (65).

520

521 **16s rDNA and ITS sequencing of community profiles**

522 To characterize microbiomes of inocula and final microbiomes of the laboratory experiments, each
523 sample was pulverized in liquid N₂, and DNA was extracted from 50 mg of material using the DNeasy
524 PowerPlant Pro Kit (Qiagen, Hilden, Germany). Extracted DNA was taken to the Genomics Core at the
525 University of Tennessee, Knoxville, for library preparation and sequencing on an Illumina MiSeq. Libraries
526 were prepped for the 16S rRNA gene using a two-step PCR approach with a mixture of custom 515F and
527 806R primers to characterize archaeal/bacterial communities, and for the *ITS2* gene region using a
528 custom mixture of primers to characterize the fungal community (66). The initial PCR consisted of 2X
529 KAPA HiFi HotStart Ready Mix Taq (Roche), 10 μ M total for each forward and reverse primer
530 combination, and approximately 50 ng of DNA. PCRs for 16S rRNA and ITS2 were performed separately.
531 Reaction conditions were as follows: 3 minutes at 95°C; 25 cycles of 95°C for 30 seconds, 55°C for 30
532 seconds, and 72°C for 30 seconds; and a final extension at 72 degrees for 5 minutes. PCR products

533 were purified using AMPure XP beads (Agencourt/Beckman Coulter, Indianapolis, IN, USA). Nextera XT
534 indexes were ligated to the PCR products via a second, reduced-cycle PCR such that each sample had a
535 unique combination of forward and reverse indexes, and the products were again purified using AMPure
536 XP beads. Samples were pooled in equal concentrations and sequenced on the MiSeq along with
537 negative control samples.

538 Microbial sequences were processed with QIIME 2 v 2018.11 platform (67). Paired sequences
539 were demultiplexed with the plugin demux and quality-filtered (denoised, dereplicated, chimera-filtered,
540 and pair-end merged) and processed into Sequence Variants (SVs) with the dada2 plugin (68).
541 Taxonomy was assigned using a pre-trained Naive Bayes classifier based on Greengenes v13_8 (99%
542 OTUs) that are trimmed to the 515F/806R primer pair for 16S rDNA and based on the UNITE (99%
543 OTUs) for ITS2. Sequences assigned as chloroplast or mitochondria were removed. Microbial diversity
544 was calculated based on a subsample of 19,000 sequences to fit the size of the smallest library. SV-
545 based alpha diversity (Shannon diversity) and beta diversity (Bray-Curtis) were calculated using the
546 phyloseq 1.30.0 (69) package in R (65). Beta diversity was visualized using nonmetric multidimensional
547 scaling ordination (NMDS) based on Bray-Curtis similarity distances. A permutational multivariate
548 analysis of variance (PERMANOVA) with 999 permutations was used to calculate the significance of
549 clustering of samples by microbial and chamber treatment. Microbial diversity correlation with *Sphagnum*
550 growth were assessed using Pearson correlation.

551

552 **Metagenomics of the starting inoculum**

553 DNA for metagenomics was extracted using a modified CTAB method (70). The ambient- and warming-
554 conditioned microbiome samples were sequenced as an Illumina TruSeq PCR-Free library on an Illumina
555 2500 in Rapid Run mode (paired-end, 2 × 150 nt). Raw sequences were processed using Atropos v.
556 1.1.17 (71) in Python v3.6.2 to remove adapter contamination and quality trimming. Quality trimming was
557 performed at the Q20 level with read pairs, and if either read of a pair was < 75 bp after adapter removal
558 and quality trimming, the read pair was discarded. Before metagenome assembly, we removed reads
559 mapping to either the *S. angustifolium* or PhiX genomes using bbmap v38.22. The remaining
560 metagenome reads for the ambient and warming samples were co-assembled using MEGAHIT v1.1.3

561 (72, 73) with default settings except --min-contig-len was set to 300. Trimmed paired-end reads were
562 mapped to the MEGAHIT co-assembly with BamM v1.7.3 (<http://ecogenomics.github.io/BamM/>) (74).
563 Putative genomes were binned from the co-assembled contigs using MetaBAT v2.12.1 (75) with –
564 minContig set to 2000. Metagenome-assembled genomes (MAGs) were assessed for completeness,
565 contamination, and strain contamination using checkM v1.0.12 (40). MAGs that were \geq 70% complete with
566 \leq 5% contamination were kept for downstream analyses. To determine differences in the relative
567 abundance of MAGs between ambient and warming metagenome samples, trimmed metagenomic reads
568 were mapped to MAGs using BamM v.1.7.3 and normalized as counts per million mapped reads. Gene
569 models were predicted for the co-assembled metagenomic contigs using Prodigal v2.6.3 (76) in
570 anonymous mode, and MAGs were annotated using prokka v1.14.0 (77). Taxonomy was assigned to
571 gene models using the lowest common ancestor algorithm implemented in DIAMOND v0.9.22 (41).
572 Inferred amino acid sequences were searched against the NCBI non-redundant protein database
573 (downloaded October 3, 2019) using default settings in DIAMOND BLASTp except as follows: --query-
574 cover 85, --top 5, and --sensitive.

575

576 **Phylogenetic Analysis of Cyanobacterial MAGs**

577 We downloaded 109 cyanobacterial RefSeq genomes from NCBI representing the currently sequenced
578 diversity of clade A (*Oscillatoria/Arthospira*) and clade B (*Nostoc/Anabaena/Cyanothece*), following the
579 nomenclature of (43), and two outgroup taxa, *Acaryochloris* sp. CCME 5410 and *A. marina* MBIC11017.
580 Additionally, we included six cyanobacterial isolates sequenced in (42), *Nostoc* moss6, *N. moss3*, *N.*
581 *moss2*, *N. moss4*, *N. moss5*, and *N. sp.* 996, six MAGs from our metagenomic assembly labeled bin14,
582 bin192, bin238, bin354, bin377, and bin384, and three binned genomes from the SPRUCE site, but
583 outside the enclosures labeled bin109, bin297, and bin367. A concatenated alignment of inferred amino
584 acids sequences from 31 proteins for the 125 cyanobacterial genomes was generated and trimmed using
585 the AMPORA2 pipeline (78). Alignment sites containing only gaps and ambiguous characters were
586 removed using FAST v1.6 (79). Molecular evolution model selection was performed with ModelFinder
587 (80). Phylogenetic analysis was conducted with IQ-TREE v1.6.8 (81) using the cpREV+C60+F+R6

588 model. Node support was evaluated using 1000 SH-like approximate likelihood ratio test (82) replicates
589 and 1000 UFboot2 replicates (81).

590

591 **Metatranscriptomics Profiling**

592 Cryogenically stored samples from the end of the experiment were ground in liquid nitrogen, and total
593 RNA was extracted using a method combining CTAB lysis buffer and the Spectrum Total Plant RNA
594 extraction kit (Sigma, Darmstadt, Germany) as described previously (83). RNA quality and quantity were
595 determined using a NanoDrop Spectrophotometer (Thermo Scientific, Waltham, MA, USA). Total RNA (3
596 µg) of three biological replicates was sent to Macrogen (Seoul, South Korea), where libraries were
597 prepared and sequenced on an Illumina HiSeq.

598 Metatranscriptome reads were partitioned into *S. angustifolium* and microbial transcripts by
599 mapping reads to the *S. angustifolium* v1.0 genome using bbmap v38.22. Microbial transcripts were
600 processed using the SAMSA v2.2.0 pipeline (84), except that differential expressed SEED functional
601 gene ontologies (85) were identified using limma-voom v3.11(86) with multiple testing correction using
602 FDR. Taxonomic classification of microbial transcripts was performed by mapping reads to the
603 metagenome assembly using BamM v1.7.3 and transferring the taxonomic classification of metagenomic
604 gene models and MAG assignments to mapped transcripts.

605 To identify differentially expressed (DE) *S. angustifolium* genes, *S. angustifolium* read-pairs were
606 mapped to *S. angustifolium* v1.0 reference genome using RSubread v2.3.0 (87) and analyzed using
607 limma-voom v3.11. Enrichment of MapMan4 ontology bins (88) in the set of DE genes was determined
608 using the MapMan desktop application v3.6.0RC1 (89). Statistical significance of MapMan ontology bins
609 was determined using Kruskal-Wallis test with multiple testing correction using FDR in R v3.6.1. Log₂(fold
610 change) (LFC) of MapMan4 ontology bins were determined by averaging LFC across DE genes within
611 each bin.

612

613 **Data Availability**

614 Raw 16S and ITS sequence files can be found on NCBI using the BioProject ID PRJNA644113. Raw
615 metagenome and metatranscriptome sequence files can be found on NCBI using the BioProject ID
616 PRJNA644538.

617

618 **Acknowledgements**

619 We are grateful for pre-submission comments from Dr. Gustaf Granath and field site maintenance from
620 Robert Nettles III. Collection of starting microbial inocula was made possible through the SPRUCE
621 project, which is supported by Office of Science; Biological and Environmental Research (BER); US
622 Department of Energy (DOE), Grant/Award Number: DE-AC05-00OR22725. Experimentation, sample
623 collection, and analyses were supported by the DOE BER Early Career Research Program. This research
624 used resources of the Compute and Data Environment for Science (CADES) at the Oak Ridge National
625 Laboratory. Oak Ridge National Laboratory is managed by UT-Battelle, LLC, for the US DOE under
626 contract no. DE-AC05-00OR22725. AJS was supported by NSF DEB-1737899, 1928514. The work
627 conducted by the US DOE Joint Genome Institute (JGI) is supported by the Office of Science of the US
628 Department of Energy under Contract No. DE-AC02-05CH11231. We thank the DOE JGI and
629 collaborators for pre-publication access to the *S. angustifolium* (formerly *S. fallax*) genome sequence.

630 **REFERENCES**

631 1. van Breemen N, Nations U, Use I (1995) How Sphagnum bogs down other plants. *Trends Ecol Evol (Personal Ed* 10(7):270–275.

632 2. Clymo RS, Hayward PM (1982) The Ecology of Sphagnum. *Bryophyte Ecology* (Springer Netherlands), pp 229–289.

633 3. Yu Z, Loisel J, Brosseau DP, Beilman DW, Hunt SJ (2010) Global peatland dynamics since the Last Glacial Maximum. *Geophys Res Lett* 37(13):1–5.

634 4. Gorham E (1991) Northern peatlands: role in the carbon cycle and probable responses to climatic warming. *Ecol Appl* 1(2):182–195.

635 5. Dorrepaal E, et al. (2003) Summer warming and increased winter snow cover affect Sphagnum fuscum growth , structure and production in a sub-arctic bog. *Glob Chang Biol* 10(1):93–104.

636 6. Robroek BJM, Limpens J, Breeuwer A, Schouten MGC (2007) Effects of water level and temperature on performance of four Sphagnum mosses. *Plant Ecol* 190(1):97–107.

637 7. Gunnarsson U, Granberg G, Nilsson M (2004) Growth, production and interspecific competition in Sphagnum: effects of temperature, nitrogen and sulphur treatments on a boreal mire. *New Phytol* 163(2):349–359.

638 8. Robroek BJM, Limpens J, Breeuwer A, Crushell PH, Schouten MGC (2007) Interspecific competition between Sphagnum mosses at different water tables. *Funct Ecol* 21(4):805–812.

639 9. Bragazza L (2008) A climatic threshold triggers the die-off of peat mosses during an extreme heat wave. *Glob Chang Biol* 14(11):2688–2695.

640 10. Bragazza L, et al. (2016) Persistent high temperature and low precipitation reduce peat carbon accumulation. *Glob Chang Biol* 22(12):4114–4123.

641 11. Norby RJ, Childs J, Hanson PJ, Warren JM (2019) Rapid loss of an ecosystem engineer: Sphagnum decline in an experimentally warmed bog. *Ecol Evol* 9(September):12571–12585.

642 12. Kostka JE, et al. (2016) The Sphagnum microbiome: New insights from an ancient plant lineage. *New Phytol* 211(1):57–64.

643 13. Weston DJ, et al. (2014) Sphagnum physiology in the context of changing climate: emergent influences of genomics, modelling and host-microbiome interactions on understanding ecosystem

658 function. *Plant Cell Environ*:n/a-n/a.

659 14. Lindo Z, Nilsson MC, Gundale MJ (2013) Bryophyte-cyanobacteria associations as regulators of
660 the northern latitude carbon balance in response to global change. *Glob Chang Biol* 19(7):2022–
661 2035.

662 15. Berg A, Danielsson Å, Svensson BH (2013) Transfer of fixed-N from N₂-fixing cyanobacteria
663 associated with the moss Sphagnum riparium results in enhanced growth of the moss. *Plant Soil*
664 362(1–2):271–278.

665 16. Basilier K (1979) Moss-Associated Nitrogen Fixation in Some Mire and Coniferous Forest
666 Environments around Uppsala, Sweden. *Lindbergia* 5(2):84–88.

667 17. Basilier K, Granhall U, Stenström T-A (1978) Nitrogen Fixation in Wet Minerotrophic Moss
668 Communities of a Subarctic Mire. *Oikos* 31(2):236.

669 18. Basilier K (1980) Fixation and Uptake of Nitrogen in Sphagnum Blue-Green Algal Associations.
670 *Oikos* 34(2):239.

671 19. Granhall ULF, Hofsten A V (1976) Nitrogenase Activity in Relation to Intracellular Organisms in
672 Sphagnum Mosses. *Physiol Plant* 36:88–94.

673 20. Vile M a., et al. (2014) N₂-fixation by methanotrophs sustains carbon and nitrogen accumulation in
674 pristine peatlands. *Biogeochemistry*. doi:10.1007/s10533-014-0019-6.

675 21. Larmoia T, et al. (2014) Methanotrophy induces nitrogen fixation during peatland development.
676 *Proc Natl Acad Sci U S A* 111(2):734–739.

677 22. Liebner S, Svenning MM (2013) Environmental transcription of *mmoX* by methane-oxidizing
678 Proteobacteria in a subarctic palsa peatland. *Appl Environ Microbiol* 79(2):701–706.

679 23. Kip N, Winden J van, Pan Y (2010) Global prevalence of methane oxidation by symbiotic bacteria
680 in peat-moss ecosystems. *Nat Geosci* 3(August):617–621.

681 24. Raghoebarsing AA, et al. (2005) Methanotrophic symbionts provide carbon for photosynthesis in
682 peat bogs. *Nature* 436(7054):1153–1156.

683 25. Lamentowicz M, Mitchell EAD (2005) The ecology of testate amoebae (protists) in Sphagnum in
684 north-western Poland in relation to peatland ecology. *Microb Ecol* 50(1):48–63.

685 26. Jassey VEJJ, et al. (2015) An unexpected role for mixotrophs in the response of peatland carbon

686 cycling to climate warming. *Sci Rep* 5(November):16931.

687 27. Stough JMA, Kolton M, Kostka JE, Weston DJ, Pelletier DA (2018) crossm Diversity of Active Viral

688 Infections within the Sphagnum Microbiome. 84(23):1–16.

689 28. Carrell AA, et al. (2019) Experimental warming alters the community composition, diversity, and N

690 2 fixation activity of peat moss (*Sphagnum fallax*) microbiomes . *Glob Chang Biol* (May):2993–

691 3004.

692 29. Heath KD, Stock AJ, Stinchcombe JR (2010) Mutualism variation in the nodulation response to

693 nitrate. *J Evol Biol* 23(11):2494–2500.

694 30. Baker DM, Freeman CJ, Wong JCY, Fogel ML, Knowlton N (2018) Climate change promotes

695 parasitism in a coral symbiosis. *ISME J* 12(3):921–930.

696 31. Cunning R, Silverstein RN, Baker a. C (2015) Investigating the causes and consequences of

697 symbiont shuffling in a multi-partner reef coral symbiosis under environmental change. *Proc R Soc*

698 *B Biol Sci* 282(1809):20141725–20141725.

699 32. Bay LK, Doyle J, Logan M, Berkelmans R, Bay LK (2016) Recovery from bleaching is mediated by

700 threshold densities of background thermo-tolerant symbiont types in a reef-building coral. *R Soc*

701 *open Sci* 3(6):160322.

702 33. Howells EJ, Abrego D, Meyer E, Kirk NL, Burt JA (2016) Host adaptation and unexpected

703 symbiont partners enable reef-building corals to tolerate extreme temperatures. *Glob Chang Biol*

704 22(8):2702–2714.

705 34. Rodriguez RJ, et al. (2008) Stress tolerance in plants via habitat-adapted symbiosis. *ISME J*

706 2(4):404–16.

707 35. Giauque H, Connor EW, Hawkes C V. (2019) Endophyte traits relevant to stress tolerance,

708 resource use and habitat of origin predict effects on host plants. *New Phytol* 221(4):2239–2249.

709 36. Redman RS, et al. (2011) Increased fitness of rice plants to abiotic stress via habitat adapted

710 symbiosis: A strategy for mitigating impacts of climate change. *PLoS One* 6(7):1–10.

711 37. Giauque H, Hawkes C V. (2013) Climate affects symbiotic fungal endophyte diversity and

712 performance. *Am J Bot* 100(7):1435–1444.

713 38. Hanson PJ, et al. (2016) Intermediate-scale community-level flux of CO₂ and CH₄ in a Minnesota

714 peatland: putting the SPRUCE project in a global context. *Biogeochemistry* 129(3):255–272.

715 39. Bowers RM, et al. (2017) Minimum information about a single amplified genome (MISAG) and a
716 metagenome-assembled genome (MIMAG) of bacteria and archaea. *Nat Biotechnol* 35(8):725–
717 731.

718 40. Parks DH, Imelfort M, Skennerton CT, Hugenholtz P, Tyson GW (2015) CheckM: Assessing the
719 quality of microbial genomes recovered from isolates, single cells, and metagenomes. *Genome*
720 *Res* 25(7):1043–1055.

721 41. Buchfink B, Xie C, Huson DH (2014) Fast and sensitive protein alignment using DIAMOND. *Nat*
722 *Methods* 12(1):59–60.

723 42. Warshan D, et al. (2017) Feathermoss and epiphytic Nostoc cooperate differently: expanding the
724 spectrum of plant–cyanobacteria symbiosis. *ISME J*:1–13.

725 43. Shih PM, et al. (2013) Improving the coverage of the cyanobacterial phylum using diversity-driven
726 genome sequencing. *Proc Natl Acad Sci U S A* 110(3):1053–1058.

727 44. Cavicchioli R, et al. (2019) Scientists' warning to humanity: microorganisms and climate change.
728 *Nat Rev Microbiol* 17(September). doi:10.1038/s41579-019-0222-5.

729 45. Redman RS, Sheehan KB, Stout RG, Rodriguez RJ, Henson JM (2002) Thermotolerance
730 Generated by Plant/Fungal Symbiosis. *Science* (80-) 298(5598):1581–1581.

731 46. Moya A, Ferrer M (2016) Functional Redundancy-Induced Stability of Gut Microbiota Subjected to
732 Disturbance. *Trends Microbiol* 24(5):402–413.

733 47. Burke C, Steinberg P, Rusch D, Kjelleberg S, Thomas T (2011) Bacterial community assembly
734 based on functional genes rather than species. *Proc Natl Acad Sci U S A* 108(34):14288–14293.

735 48. Apprill A (2020) The Role of Symbioses in the Adaptation and Stress Responses of Marine
736 Organisms. *Ann Rev Mar Sci* 12(1):291–314.

737 49. Ziegler M, Seneca FO, Yum LK, Palumbi SR, Voolstra CR (2017) Bacterial community dynamics
738 are linked to patterns of coral heat tolerance. *Nat Commun* 8:1–8.

739 50. Larkindale J, Mishkind M, Vierling E (2007) Plant Responses to High Temperature. *Plant Abiotic*
740 *Stress*:100–144.

741 51. Mclellan CA, et al. (2007) A Rhizosphere Fungus Enhances Arabidopsis Thermotolerance through

742 Production of an HSP90 Inhibitor 1. doi:10.1104/pp.107.101808.

743 52. Clarke SM, et al. (2009) Jasmonates act with salicylic acid to confer basal thermotolerance in

744 *Arabidopsis thaliana*. *New Phytol* 182(1):175–187.

745 53. Yamamoto Y, et al. (2015) Functional analysis of allene oxide cyclase, MpAOC, in the liverwort

746 *Marchantia polymorpha*. *Phytochemistry* 116(1):48–56.

747 54. Huang J, et al. (2010) Functional analysis of the *Arabidopsis* PAL gene family in plant growth,

748 development, and response to environmental stress. *Plant Physiol* 153(4):1526–1538.

749 55. Kotak S, et al. (2007) Complexity of the heat stress response in plants. *Curr Opin Plant Biol*

750 10(3):310–316.

751 56. Conrath U, et al. (2006) Priming: Getting Ready for Battle. *Mol Plant-Microbe Interact MPMI*

752 19(10):1062–1071.

753 57. Ali SZ, et al. *Pseudomonas* sp. strain AKM-P6 enhances tolerance of sorghum seedlings to

754 elevated temperatures. doi:10.1007/s00374-009-0404-9.

755 58. Meena KK, et al. (2017) Abiotic stress responses and microbe-mediated mitigation in plants: The

756 omics strategies. *Front Plant Sci* 8:172.

757 59. Lau JA, Lennon JT (2012) Rapid responses of soil microorganisms improve plant fitness in novel

758 environments. *Proc Natl Acad Sci U S A* 109(35):14058–62.

759 60. Weston DJ, et al. (2017) The Sphagnum Project: enabling ecological and evolutionary insights

760 through a genus-level sequencing project Author Affiliations: 1–29.

761 61. Keuper F, et al. (2020) Carbon loss from northern circumpolar permafrost soils amplified by

762 rhizosphere priming. *Nat Geosci* 13(8):560–565.

763 62. Gavazov K, et al. (2018) Vascular plant-mediated controls on atmospheric carbon assimilation and

764 peat carbon decomposition under climate change. *Glob Chang Biol* 24(9):3911–3921.

765 63. Schneider CA, Rasband WS, Eliceiri KW (2012) NIH Image to ImageJ: 25 years of image analysis.

766 *Nat Methods* 9(7):671–675.

767 64. Fox J, Weisberg S (2019) *An R companion to applied regression (Third)* (Sage, Thousand Oaks

768 CA).

769 65. R Core Team (2015) R: A language and environment for statistical computing. Available at:

770 <http://www.r-project.org/>.

771 66. Cregger MA, et al. (2018) The *Populus* holobiont: Dissecting the effects of plant niches and
772 genotype on the microbiome. *Microbiome* 6(1):1–14.

773 67. Bolyen E, et al. (2019) Reproducible, interactive, scalable and extensible microbiome data science
774 using QIIME 2. *Nat Biotechnol* 37(8):852–857.

775 68. Callahan BJ, et al. (2016) DADA2: High-resolution sample inference from Illumina amplicon data.
776 *Nat Methods* 13(7):581–583.

777 69. McMurdie PJ, Holmes S (2013) phyloseq: An R Package for Reproducible Interactive Analysis and
778 Graphics of Microbiome Census Data. *PLoS One* 8(4):e61217.

779 70. Carrell AA, Frank AC (2014) *Pinus flexilis* and *Picea engelmannii* share a simple and consistent
780 needle endophyte microbiota with a potential role in nitrogen fixation. *Front Microbiol* 5(JULY):1–
781 11.

782 71. Didion JP, Martin M, Collins FS (2017) Atropos: Specific, sensitive, and speedy trimming of
783 sequencing reads. *PeerJ* 2017(8):1–19.

784 72. Li D, et al. (2016) MEGAHIT v1.0: A fast and scalable metagenome assembler driven by
785 advanced methodologies and community practices. *Methods* 102:3–11.

786 73. Li D, Liu CM, Luo R, Sadakane K, Lam TW (2015) MEGAHIT: An ultra-fast single-node solution
787 for large and complex metagenomics assembly via succinct de Bruijn graph. *Bioinformatics*
788 31(10):1674–1676.

789 74. Li H, Durbin R (2009) Fast and accurate short read alignment with Burrows-Wheeler transform.
790 *25(14):1754–1760.*

791 75. Kang DD, et al. (2019) MetaBAT 2: an adaptive binning algorithm for robust and efficient genome
792 reconstruction from metagenome assemblies. *PeerJ* 7:e7359.

793 76. Hyatt D, et al. (2010) *Prodigal: prokaryotic gene recognition and translation initiation site*
794 *identification* Available at: <http://www.biomedcentral.com/1471-2105/11/119> [Accessed July 6,
795 2020].

796 77. Seemann T (2014) Genome analysis Prokka: rapid prokaryotic genome annotation. *30(14):2068–*
797 *2069.*

798 78. Wu M, Scott AJ (2012) Phylogenomic analysis of bacterial and archaeal sequences with
799 AMPHORA2. *Bioinforma Appl NOTE* 28(7):1033–1034.

800 79. Lawrence TJ, et al. (2015) FAST: FAST Analysis of Sequences Toolbox. *Front Genet* 6(MAY):172.

801 80. Kalyaanamoorthy S, Minh BQ, Wong TKF, Von Haeseler A, Jermiin LS (2017) ModelFinder: Fast
802 model selection for accurate phylogenetic estimates. *Nat Methods* 14(6):587–589.

803 81. Quang B, Anh M, Nguyen T, Von Haeseler A Ultrafast Approximation for Phylogenetic Bootstrap.
804 doi:10.1093/molbev/mst024.

805 82. St' S, et al. (2010) New Algorithms and Methods to Estimate Maximum-Likelihood Phylogenies:
806 Assessing the Performance of PhyML 3.0. *Syst Biol* 59(3):307–321.

807 83. Timm CM, et al. (2016) Two poplar-associated bacterial isolates induce additive favorable
808 responses in a constructed plant-microbiome system. *Front Plant Sci* 7(APR2016):1–10.

809 84. Westreich ST, Korf I, Mills DA, Lemay DG (2016) SAMSA: a comprehensive metatranscriptome
810 analysis pipeline. doi:10.1186/s12859-016-1270-8.

811 85. Overbeek R, et al. The SEED and the Rapid Annotation of microbial genomes using Subsystems
812 Technology (RAST). doi:10.1093/nar/gkt1226.

813 86. Ritchie ME, et al. (2015) limma powers differential expression analyses for RNA-sequencing and
814 microarray studies. *Nucleic Acids Res* 43(7). doi:10.1093/nar/gkv007.

815 87. Liao Y, Smyth GK, Shi W (2019) The R package Rsubread is easier, faster, cheaper and better for
816 alignment and quantification of RNA sequencing reads. *Nucleic Acids Res* 47(8).
817 doi:10.1093/nar/gkz114.

818 88. Schwacke R, et al. (2019) MapMan4: A Refined Protein Classification and Annotation Framework
819 Applicable to Multi-Omics Data Analysis. *Mol Plant* 12:879–892.

820 89. Thimm O, et al. (2004) mapman: a user-driven tool to display genomics data sets onto diagrams of
821 metabolic pathways and other biological processes. *Plant J* 37(6):914–939.

822